AIAA JOURNAL
Vol. 39, No. 10, October 2001

Partially Implicit Scheme for Chemically Reacting Flows at All Mach Numbers

Seong-Lyong Kim* and In-Seuck Jeung†
Seoul National University, Seoul 151-742, Republic of Korea
and
Yun-Ho Choi‡
Ajou University, Suwon 442-749, Republic of Korea

Chemical reactions make computations of chemically reacting flows stiff. The degree of stiffness increases as the Mach number decreases because the flow timescale increases while the reaction timescales remain constant. Thus, the computation of reacting flows at low Mach numbers is more difficult than that in high Mach number. In the present study a new implicit scheme that employs partially implicit treatment of chemical source terms at mixed time levels has been developed. The chemical Jacobian is reduced to a partial form of the full chemical Jacobian (a lower triangular matrix) and thus saves time in matrix inversion. In addition, robust calculation of the reacting flows is made possible because a negative real eigenvalue of the partial chemical Jacobian allows larger time-step sizes than the full chemical Jacobian. For applications at all Mach numbers, a preconditioned lower upper symmetric Gauss–Seidel scheme employing an approximate flux Jacobian splitting is incorporated. For high-Mach-number flows the partially implicit scheme maintains similar convergence rates to the fully implicit one; therefore, it enhances computational efficiency by reducing computing time per iteration. For low-Mach-number reacting flows it also enables robust calculation of reactions as well as the fully implicit one; however, its convergence rate is rather slow. Furthermore, more stable and efficient computations are possible when the fully implicit scheme is coupled with the partially implicit one.

Nomenclature

$\boldsymbol{A}$	=	flux Jacobian for the ξ direction
$\boldsymbol{A}^{\pm}$	=	flux-split Jacobian for the ξ direction
$\boldsymbol{B}$	=	flux Jacobian for the η direction
$\boldsymbol{B}^{\pm}$	=	flux-split Jacobian for the η direction
C_i	=	mole concentration of species i
C_p	=	coefficient of specific heat at constant pressure
$C_{v,i}$	=	coefficient of specific heat at constant volume for species i
c	=	sonic speed
$\boldsymbol{E}$	=	convective flux in the ξ direction
$\boldsymbol{E}_v$	=	viscous flux in the ξ direction
$\boldsymbol{F}$	=	convective flux in the η direction
$\boldsymbol{F}_v$	=	viscous flux in the η direction
H	=	total enthalpy
$\boldsymbol{H}$	=	axisymmetric convective flux
$\boldsymbol{H}_v$	=	axisymmetric viscous flux
h_i	=	static enthalpy of species i
J	=	Jacobian of grid transformation
k	=	turbulent kinetic energy
$k_{b,k}$	=	backward reaction rate for the kth reaction
$k_{f,k}$	=	forward reaction rate for the kth reaction
$L_{1,j}$	=	chemical first loss term
$L_{2,j}$	=	chemical second loss term
M	=	Mach number
$\boldsymbol{M}$	=	modal matrix of flux Jacobian
NR	=	total number of reaction steps
NS	=	total number of species
p	=	pressure
p_{atm}	=	atmospheric pressure
p_g	=	gauge pressure
Q_i	=	chemical production term
$\boldsymbol{Q}$	=	primary dependent vector
R	=	gas constant
$\boldsymbol{R}$	=	full chemical Jacobian matrix
$\boldsymbol{R}_p$	=	partial chemical Jacobian matrix
T	=	gas temperature
t	=	time
U	=	contravariant velocity in the ξ direction
u	=	velocity in the x direction
V	=	contravariant velocity in the η direction
$\boldsymbol{V}$	=	viscous flux Jacobian
v	=	velocity in the y direction
$\boldsymbol{W}$	=	source term vector
Y_i	=	mass fraction of species i
Γ	=	preconditioning matrix
ε	=	turbulent dissipation rate
ε_i	=	internal energy of species i
ε_p	=	preconditioning parameter
κ	=	dissipation parameter
$\nu_{j,k}$	=	stoichiometric coefficient of species j for reaction k
ξ, η	=	generalized coordinates
ρ	=	density
ω_i	=	finite rate source term for species i

Subscripts and Superscripts

i	=	index for the ξ direction and species
j	=	index for the η direction and species
k	=	index for reaction
n	=	index for iteration count

Received 29 August 2000; revision received 4 May 2001; accepted for publication 6 May 2001.

*Graduate Research Assistant, Department of Aerospace Engineering, San 56-1 Shinlim-dong Kwanak-ku; lyongkim@gong.snu.ac.kr.

†Professor, Department of Aerospace Engineering, San 56-1 Shinlim-dong Kwanak-ku; enjis@snu.ac.kr. Senior Member AIAA.

‡Professor, Department of Mechanical Engineering, Wonchon-dong Paldal-ku; ychoi@ madang.ajou.ac.kr. Member AIAA.

Introduction

THE computation of chemically reacting flows shows stiffness caused by chemical reactions. The chemical stiffness arises because of difference between characteristic timescales. A large spectrum of timescales appears as reactions evolve, and chemical timescales are generally smaller than the flow timescales. The difference between chemical and flow timescales has a direct relation with the Mach number because the chemical timescales remain constant,

whereas the flow timescales increase as the Mach number decreases. This chemical stiffness forces implicit treatment of chemical source terms.

However, the implicit treatment of the chemical source terms incurs difficulties in numerical computation. First, the eigenvalues of the chemical Jacobian sometimes show positive real eigenvalues, which can cause numerical instability.[1] Also, there is an inherent disadvantage of additional computational time in matrix inversion. In particular, in the lower–upper symmetric Gauss–Seidel (LU-SGS) scheme employing approximate flux Jacobian splitting[2] its innate merit of "matrix-free" manipulation disappears. Therefore, an improved method capable of maintaining the numerical stability as well as facilitating computational efficiency has been required. For this purpose present study incorporates an approximate chemical Jacobian and also applied a preconditioned scheme that modifies the time-derivative terms of equations so that the difference between flow and acoustic timescales remains bounded in the computation of low-Mach-number flows.

To enhance numerical efficiency of the LU-SGS scheme, several simplified chemical Jacobians have recently been suggested.[3–5] Among them, Eberhardt and Imlay[3] derive a diagonalized chemical Jacobian that has the form of a diagonal matrix, whose diagonal terms are the L_2 norms of the full chemical Jacobian. Edwards[4] also suggests a column-wise approximate factorization procedure for the chemical Jacobian matrix. Their study shows efficiency gain in high-Mach-number flows. Kim et al.[5] introduce two types of partial chemical Jacobian by treating the chemical source terms at mixed time levels. In this approach the chemical source terms are treated in a partially implicit fashion. They also apply partial chemical Jacobians to constant volume reaction and shock-induced combustion.

The preceding methods, however, have been applied only in supersonic reacting flows. In subsonic reacting flows the computation of reacting flows is more difficult because the discrepancy between flow and chemical timescales is larger. Furthermore, the positive eigenvalues of the chemical Jacobian matrix sometimes aggravate the efficiency of implicit schemes. Accordingly, this study presents a partially implicit preconditioned LU-SGS scheme for computing a wide range of Mach-number reacting flows by incorporating the partial Jacobian concept. In addition, it is shown that the present method can be used for robust treatment of the instability because of the positive eigenvalues that arises in many low-Mach-number reacting flow computations.

First, a constant volume reaction is considered to examine the accuracy and the effects of the partial Jacobian on the chemical stiffness. Then the preconditioning technique of Venkateswaran et al.[6] is applied to the partially implicit technique for efficient computation of reacting flows at all speeds. Four test cases—a shock-induced combustion of Lehr,[7] a planar reacting shear layer measured by Chang et al.,[8] a laminar hydrogen air flame of Fukutani et al.,[9] and a laminar methane air flame of Mitchell et al.[10]—are investigated to validate the present method. The convergence histories and time-step limitations of the partially implicit scheme are also illustrated and compared with those of the fully implicit one.

Partially Implicit Treatment of Chemical Source Terms

In this section the partial Jacobians are derived and applied to a constant volume reaction. In a fully implicit scheme the chemical source terms are evaluated at the advanced $(n+1)$ time level. On the other hand, the partially implicit scheme needs some of the $(n+1)$ time level values to be evaluated at the (n) time level, and thus $(n+1)$ and (n) time levels are simultaneously used for the evaluation of chemical source terms. Such mixed time levels result in partial chemical Jacobians, subsets of the full chemical Jacobian. Among many partial chemical Jacobians, two of them are mathematically important:

$$\omega_i = \omega_i\left(Y_1^{n+1}, \ldots, Y_i^{n+1}, Y_{i+1}^{n}, \ldots, Y_{\mathrm{NS}}^{n}\right) \approx \omega_i\left(Y_1^{n}, \ldots, Y_{\mathrm{NS}}^{n}\right) + \sum_{j=1}^{i} \frac{\partial \omega_i}{\partial Y_j}\left(Y_j^{n+1} - Y_j^{n}\right) \tag{1}$$

$$\omega_i = \omega_i\left(Y_1^{n}, \ldots, Y_{i-1}^{n}, Y_i^{n+1}, Y_{i+1}^{n}, \ldots, Y_{\mathrm{NS}}^{n}\right) \approx \omega_i\left(Y_1^{n}, \ldots, Y_{\mathrm{NS}}^{n}\right) + \frac{\partial \omega_i}{\partial Y_i}\left(Y_i^{n+1} - Y_i^{n}\right) \tag{2}$$

The rightmost term of Eqs. (1) and (2) represent the Gauss–Seidel and Jacobi partial chemical Jacobians whose names originate from iterative methods[5] and have the forms of a lower triangular matrix and a diagonal matrix, respectively.

The Gauss–Seidel partial chemical Jacobian of Eq. (1) can have different components depending on the species ordering. The species ordering is determined through a linear stability analysis.[5] Therefore radical species such as H, O, HO_2, and H_2O_2 should be located in the rear part of the primary dependent vector. However, the species ordering may not affect the performance of the partial chemical Jacobian if the time-step size is the same as that of the scheme with the full chemical Jacobian.

In the present study the species ordering is chosen to be {H_2, O_2, OH, H_2O, H, O, HO_2, H_2O_2}, which is the same as in the previous research.[5] Here, only the Gauss–Seidel partial chemical Jacobian is used because of the time-step limitation of the Jacobi partial chemical Jacobian.[5] Hereafter, the Gauss–Seidel partial chemical Jacobian is referred to as the partial chemical Jacobian and the scheme with the partial chemical Jacobian as the partially implicit scheme. In a similar sense the scheme with the diagonalized chemical Jacobian is referred to as the diagonally implicit scheme.

As a representative of a constant volume reaction, the adiabatic hydrogen–oxygen reaction is selected. Initial conditions are set to 10 atm and 1200 K. The chemistry mechanism used in this case is GRI Mech. V2.11 (data available on-line at http://www.me.berkeley.edu/gri-mech/) including eight species and 24 reaction steps model. The governing equations for constant volume reactions are given as

$$\frac{\mathrm{d}C_i}{\mathrm{d}t} = \omega_i = \sum_{k=1}^{\mathrm{NR}} (\nu''_{i,k} - \nu'_{i,k}) \left\{ k_{f,k} \prod_{j=1}^{\mathrm{NS}} C_j^{\nu'_{j,k}} - k_{b,k} \prod_{j=1}^{\mathrm{NS}} C_j^{\nu''_{j,k}} \right\} \tag{3a}$$

$$\frac{\mathrm{d}T}{\mathrm{d}t} = \frac{-\sum \varepsilon_i \omega_i}{\sum C_i C_{v,i}} \tag{3b}$$

The discretized form of the equations is as follows:

$$(1/\Delta t - \boldsymbol{R})^n \Delta \boldsymbol{Y}^{n+1} = \boldsymbol{f}^n, \qquad \Delta \boldsymbol{Y}^{n+1} = \boldsymbol{Y}^{n+1} - \boldsymbol{Y}^n \tag{4a}$$

where

$$\boldsymbol{Y} = [C_1, \ldots C_{\mathrm{NS}}, T]^T \tag{4b}$$

and $\boldsymbol{f}$ is the source term vector including the species and energy sources. The full chemical Jacobian $\boldsymbol{R}$ is replaced by the partial chemical Jacobian $\boldsymbol{R}_p$, when the partially implicit scheme is used.

Figures 1a and 1b show temperature histories at various time-step sizes using partial, diagonalized, and full chemical Jacobians. With the full chemical Jacobian an accurate solution is produced with the time-step size of 10^{-2} μs, while it diverges with the time-step size above 10^{-2} μs. Figure 1 also shows that computations with Gauss–Seidel partial or diagonalized chemical Jacobians are possible at larger time-step sizes although their accuracy deteriorates at larger time-step sizes. The temperature discrepancies of the partial and diagonalized schemes with large time-step sizes can be explained by nonconservation of mass as a result of the time level inconsistency in the chemical source terms.[5] Nevertheless, Fig. 1 shows the enhanced stability of the partial and diagonalized chemical Jacobians.

The partial chemical Jacobian characteristics can be analyzed more accurately by tracing the eigenvalues of the chemical source terms, as shown in Fig. 2. The eigenvalues of the full chemical Jacobian matrix are complex, and their real parts vary from 10^2 to 10^8 as reactions progress. For time integration the sign of the eigenvalues is more important. Preferable time-integration methods differ depending on the sign of the eigenvalue.[1] For the negative real eigenvalue it should be treated in an implicit manner, whereas an explicit treatment is preferred for positive eigenvalues. If complex eigenvalues appear, explicit treatment is used only for the positive real values. In chemical reactions all types of eigenvalues appear, as shown in Fig. 2. Therefore, to obtain optimum stability the

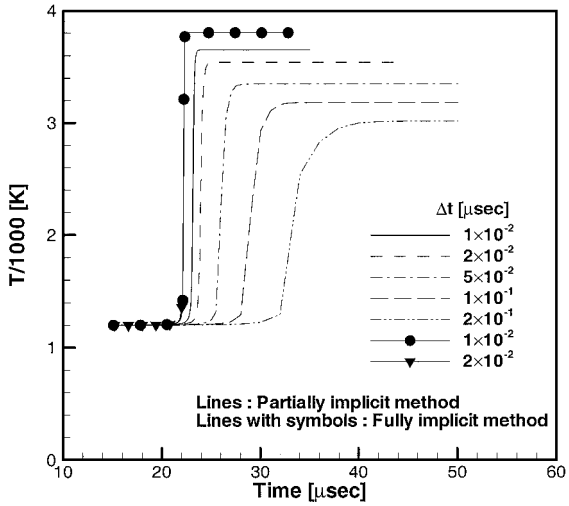

Fig. 1a Temperature time histories of the constant volume reaction with the partially implicit method.

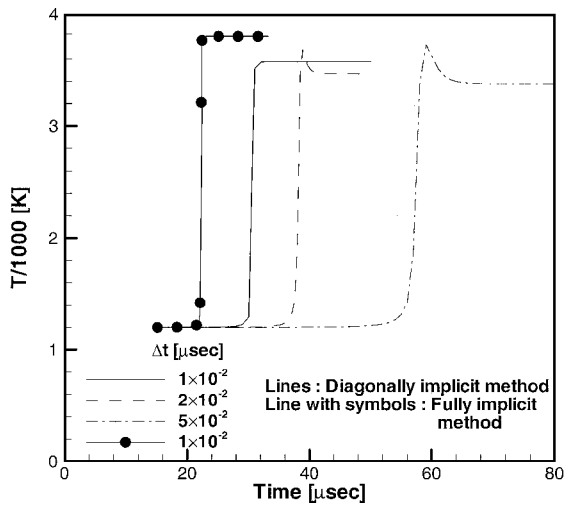

Fig. 1b Temperature time histories of the constant volume reaction with the diagonally implicit method.

chemical Jacobian matrix has to be decomposed according to the sign of the eigenvalue.[1,7] However, the Jacobian matrix splitting is time consuming because the eigenvalue signs and magnitudes vary as reactions progress. Furthermore, it is also impossible to obtain analytically the eigenvalues of the source term.

However, unlike the full chemical Jacobian, the partial chemical Jacobian has only negative real eigenvalues because of its lower triangular matrix form. This can be simply shown if the chemical source terms are rearranged as the sum of production $Q_i(Y_{j,j\neq i})$ and loss terms $Y_i L_{1,i}(Y_{j,j\neq i}) + Y_i^2 L_{2,i}(Y_{j,j\neq i})$, as follows:

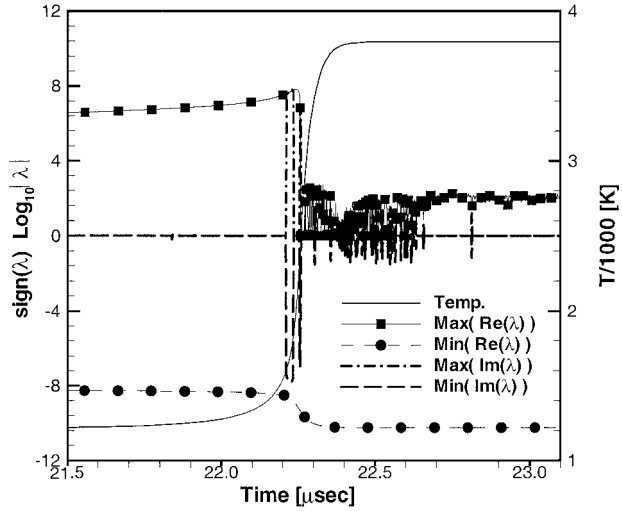

Fig. 2 Eigenvalues of the chemical Jacobian for the constant volume reaction.

$$\lambda_i(\boldsymbol{R}_p) = \frac{\partial \omega_i}{\partial Y_i} = \frac{\partial\left(Q_i - Y_i L_{1,i} - Y_i^2 L_{2,i}\right)}{\partial Y_i} = -L_{1,i} - 2Y_i L_{2,i} \tag{5}$$

Thus, the computation with the partial chemical Jacobian is more stable than that with the full chemical Jacobian and allows larger time-step sizes as shown in Fig. 1. We expect that the enhanced stability of the partial chemical Jacobian helps the robust computation of the multidimensional reacting flows.

Numerical Formulations

Among many schemes for reacting flow computations, time-derivative preconditioning methods[6,11,12] are widely used because they are able to calculate flows at all Mach numbers. In the present study the partial chemical Jacobian is incorporated into a preconditioned equation to enhance stability characteristics as well as to obtain computational capabilities over a wide range of flow conditions.

Governing Equations

The vector form of the equations of motion for turbulent chemically reacting flows in the generalized axisymmetric coordinates is as follows:

$$\Gamma\frac{\partial \boldsymbol{Q}}{\partial t} + \frac{\partial \boldsymbol{E}}{\partial \xi} + \frac{\partial \boldsymbol{F}}{\partial \eta} + \boldsymbol{H} = \frac{\partial \boldsymbol{E}_v}{\partial \xi} + \frac{\partial \boldsymbol{F}_v}{\partial \eta} + \boldsymbol{H}_v + \boldsymbol{W} \tag{6}$$

Detailed descriptions of the vectors can be found in Ref. 11.

Various preconditioning matrices[6,11,12] have been suggested for chemically reacting flows. Among them, the preconditioning matrix developed by Choi and Merkel[13] and applied to reacting flows by Venkateswaran et al.[6] is used in this study. The matrix offers time advantage in performing matrix inversion because of its lower triangular matrix form. The primary dependent vector $\boldsymbol{Q}$ and the preconditioning matrix Γ are as follows:

$$\boldsymbol{Q} = \frac{1}{J}\begin{bmatrix} p_g \\ u \\ v \\ T \\ k \\ \varepsilon \\ Y_1 \\ \vdots \\ Y_{\mathrm{NS}-1} \end{bmatrix}, \qquad \Gamma = \begin{bmatrix} 1/\varepsilon_p c^2 & 0 & 0 & 0 & 0 & 0 & 0 & \cdots & 0 \\ u/\varepsilon_p c^2 & \rho & 0 & 0 & 0 & 0 & 0 & \cdots & 0 \\ v/\varepsilon_p c^2 & 0 & \rho & 0 & 0 & 0 & 0 & \cdots & 0 \\ H/\varepsilon_p c^2 - 1 & \rho u & \rho v & \rho C_p & 5/3\rho & 0 & \rho(h_1 - h_{\mathrm{NS}}) & \cdots & \rho(h_{\mathrm{NS}-1} - h_{\mathrm{NS}}) \\ k/\varepsilon_p c^2 & 0 & 0 & 0 & \rho & 0 & 0 & \cdots & 0 \\ \varepsilon/\varepsilon_p c^2 & 0 & 0 & 0 & 0 & \rho & 0 & \cdots & 0 \\ Y_1/\varepsilon_p c^2 & 0 & 0 & 0 & 0 & 0 & \rho & \cdots & 0 \\ \vdots & \vdots & \vdots & \vdots & \vdots & \vdots & \vdots & \ddots & \vdots \\ Y_{\mathrm{NS}-1}/\varepsilon_p c^2 & 0 & 0 & 0 & 0 & 0 & 0 & \cdots & \rho \end{bmatrix} \tag{7}$$

where the gauge pressure p_g is defined as $p_g = p - p_{\text{atm}}$. For the optimum condition number the preconditioning parameter ε_p is defined as follows:

$$\varepsilon_p = \text{Min}\,[1,\ \text{Max}(M^2, 10^{-10})] \tag{8}$$

Spatial Discretization

Convective terms are expressed as differences between numerical fluxes at the cell interfaces. The numerical fluxes containing artificial dissipation are formulated using Roe's type of the flux difference splitting method.[14] The flux vector at the cell interface in ξ direction can be written as

$$\boldsymbol{E}_{i+\frac{1}{2},j} = \tfrac{1}{2}[\boldsymbol{E}(\boldsymbol{Q}_{i+1}) + \boldsymbol{E}(\boldsymbol{Q}_i) - |\boldsymbol{A}(\boldsymbol{Q}_{i+1}, \boldsymbol{Q}_i)|(\boldsymbol{Q}_{i+1} - \boldsymbol{Q}_i)] \tag{9}$$

Here, $|\boldsymbol{A}|$ implies the flux Jacobian matrix composed of absolute eigenvalues, defined as $|\boldsymbol{A}| = \boldsymbol{\Gamma M}|\boldsymbol{\Lambda}|\boldsymbol{M}^{-1}$. The detailed formulations of numerical dissipation in Eq. (9) are as follows:

$$\begin{aligned}
\boldsymbol{\Gamma M}|\boldsymbol{\Lambda}|\boldsymbol{M}^{-1}\Delta\boldsymbol{Q} = \frac{1}{J}|U|&\begin{bmatrix} 0 \\ l_x\phi_1 + \rho\Delta u \\ l_y\phi_2 + \rho\Delta v \\ \tilde{U}\phi_1 + (\rho/2)\Delta(u^2+v^2) + \frac{5}{3}\rho\Delta k \\ \rho\Delta k \\ \rho\Delta\varepsilon \\ \rho\Delta Y_i \end{bmatrix} \\
+\frac{1}{J}|U'+c'|&\begin{bmatrix} \phi_2 \\ (u + l_x\psi_1/2)\phi_2 \\ (v + l_y\psi_1/2)\phi_2 \\ (H + \tilde{U}\psi_1/2)\phi_2 \\ k\phi_2 \\ \varepsilon\phi_2 \\ Y_i\phi_2 \end{bmatrix} \\
+\frac{1}{J}|U'-c'|&\begin{bmatrix} \phi_3 \\ (u + l_x\psi_2/2)\phi_3 \\ (v + l_y\psi_2/2)\phi_3 \\ (H + \tilde{U}\psi_2/2)\phi_3 \\ k\phi_3 \\ \varepsilon\phi_3 \\ Y_i\phi_3 \end{bmatrix}
\end{aligned} \tag{10}$$

where

$$\phi_1 = \frac{\tilde{U}}{RT}\left[-\frac{R\Delta p_g}{C_p} + \rho R\Delta T + \frac{2}{3}\rho\Delta k + \sum_{1}^{\text{NS}-1}\rho(R_i - R_{\text{NS}})T\Delta Y_i\right] - \rho\Delta\tilde{U} \tag{11a}$$

$$\phi_2 = \frac{1}{s}\left[\frac{2\Delta p_g}{\tilde{U}(1-\varepsilon_p)+s} + \rho\Delta\tilde{U}\right] + \frac{\tilde{U}}{sT}\left(\frac{\Delta p_g}{C_p} - \rho\Delta T\right) - \frac{\rho\tilde{U}}{sRT}\left[\frac{2}{3}\Delta k + \sum_{1}^{\text{NS}-1}(R_i - R_{\text{NS}})T\Delta Y_i\right] \tag{11b}$$

$$\phi_3 = -\frac{1}{s}\left[\frac{2\Delta p_g}{\tilde{U}(1-\varepsilon_p)-s} + \rho\Delta\tilde{U}\right] - \frac{\tilde{U}}{sT}\left(\frac{\Delta p_g}{C_p} - \rho\Delta T\right) + \frac{\rho\tilde{U}}{sRT}\left[\frac{2}{3}\Delta k + \sum_{1}^{\text{NS}-1}(R_i - R_{\text{NS}})T\Delta Y_i\right] \tag{11c}$$

$$\psi_1 = \tilde{U}(1-\varepsilon_p) + s, \qquad \psi_2 = \tilde{U}(1-\varepsilon_p) - s \tag{11d}$$

$$s = \sqrt{\tilde{U}(1-\varepsilon_p)^2 + 4\varepsilon_p c^2} \tag{11e}$$

$$\tilde{U} = l_x u + l_y v, \qquad U = \xi_x u + \xi_y v \tag{11f}$$

$$l_x = \xi_x/|\nabla\xi|, \qquad l_y = \xi_y/|\nabla\xi| \tag{11g}$$

$$U' = \frac{1}{2}U(1+\varepsilon_p), \qquad c' = \frac{1}{2}\sqrt{U^2(1-\varepsilon_p)^2 + 4\varepsilon_p c^2\left(\xi_x^2 + \xi_y^2\right)} \tag{11h}$$

Here the modal matrix $\boldsymbol{M}$ is obtained by expanding from Buelow[15] to multispecies component. To satisfy the second law of thermodynamics, the entropy fixing function by Montagne et al.[16] is also used in the present study. To extend the upwind scheme to a higher order, the monotone upstream-centered schemes for scalar conservation laws scheme is used for the extrapolation of primitive variables at a cell interface.

Time Integration

If an Euler implicit method is used as a basic time-integration method, the value $\boldsymbol{Q}$ at the advanced time level $(n+1)$ becomes

$$\boldsymbol{\Gamma Q}^{n+1} = \boldsymbol{\Gamma Q}^n - \Delta t\left\{\frac{\partial \boldsymbol{E}}{\partial\xi} + \frac{\partial \boldsymbol{F}}{\partial\eta} - \frac{\partial \boldsymbol{E}_v}{\partial\xi} - \frac{\partial \boldsymbol{F}_v}{\partial\eta} + \boldsymbol{H} - \boldsymbol{H}_v - \boldsymbol{W}\right\}^{n+1} \tag{12}$$

By using a local Taylor-series expansion, the preceding equation can be rearranged as follows:

$$\boldsymbol{C}_{i,j}\Delta\boldsymbol{Q}_{i,j} + \boldsymbol{C}_{i-1}\Delta\boldsymbol{Q}_{i-1} + \boldsymbol{C}_{j-1}\Delta\boldsymbol{Q}_{j-1} + \boldsymbol{C}_{i+1}\Delta\boldsymbol{Q}_{i+1} + \boldsymbol{C}_{j+1}\Delta\boldsymbol{Q}_{j+1} = -\mathbf{RHS}^n \tag{13}$$

$$\begin{aligned}
\boldsymbol{C}_{i,j} = {}& \frac{\Gamma}{\Delta t} + \frac{1}{2}\left(|\boldsymbol{A}|_{i+\frac{1}{2}} + |\boldsymbol{A}|_{i-\frac{1}{2}} + |\boldsymbol{B}|_{j+\frac{1}{2}} + |\boldsymbol{B}|_{j-\frac{1}{2}}\right) \\
&+ \left(\boldsymbol{V}_{\xi\xi,i+\frac{1}{2}} + \boldsymbol{V}_{\xi\xi,i-\frac{1}{2}} + \boldsymbol{V}_{\eta\eta,j+\frac{1}{2}} + \boldsymbol{V}_{\eta\eta,j-\frac{1}{2}}\right) \\
&+ \frac{\partial \boldsymbol{H}}{\partial \boldsymbol{Q}} + \frac{\partial \boldsymbol{H}_v}{\partial \boldsymbol{Q}} + \frac{\partial \boldsymbol{W}}{\partial \boldsymbol{Q}}
\end{aligned} \tag{14a}$$

$$\boldsymbol{C}_{i-1} = -\frac{1}{2}\left(\boldsymbol{A}_{i-1} + |\boldsymbol{A}|_{i-\frac{1}{2}}\right) - \boldsymbol{V}_{\xi\xi,i-\frac{1}{2}}$$

$$\boldsymbol{C}_{j-1} = -\frac{1}{2}\left(\boldsymbol{B}_{j-1} + |\boldsymbol{B}|_{j-\frac{1}{2}}\right) - \boldsymbol{V}_{\eta\eta,j-\frac{1}{2}} \tag{14b}$$

$$\boldsymbol{C}_{i+1} = \frac{1}{2}\left(\boldsymbol{A}_{i-1} - |\boldsymbol{A}|_{i-\frac{1}{2}}\right) - \boldsymbol{V}_{\xi\xi,i-\frac{1}{2}}$$

$$\boldsymbol{C}_{j+1} = \frac{1}{2}\left(\boldsymbol{B}_{j+1} - |\boldsymbol{B}|_{j+\frac{1}{2}}\right) - \boldsymbol{V}_{\eta\eta,j+\frac{1}{2}} \tag{14c}$$

$$\mathbf{RHS} = \left\{\frac{\partial \boldsymbol{E}}{\partial\xi} + \frac{\partial \boldsymbol{F}}{\partial\eta} - \frac{\partial \boldsymbol{E}_v}{\partial\xi} - \frac{\partial \boldsymbol{F}_v}{\partial\eta} + \boldsymbol{H} - \boldsymbol{H}_v - \boldsymbol{W}\right\} \tag{14d}$$

where the ξ-directional flux Jacobians $\boldsymbol{A}$, the η-directional flux Jacobians $\boldsymbol{B}$, and the viscous flux Jacobian $\boldsymbol{V}$ are documented in Ref. 15. In the implicit terms on the left-hand side, convective terms are discretized by a first-order upwind difference method, and viscous terms are discretized by a central difference method only for $\xi\xi$ and $\eta\eta$ directions. The viscous axisymmetric Jacobian $\partial \boldsymbol{H}_v/\partial \boldsymbol{Q}$ and the species components of the inviscid axisymmetric Jacobian $\partial \boldsymbol{H}/\partial \boldsymbol{Q}$ are not considered in current calculations. The absolute flux Jacobian $|\boldsymbol{A}|$ is replaced by its maximum eigenvalue,[2]

$$|\boldsymbol{A}| = \kappa\lambda_{\max}(\Gamma^{-1}\boldsymbol{A})\Gamma, \qquad \kappa \geq 1 \tag{15}$$

Thus, except for the chemical Jacobian $\partial \boldsymbol{W}/\partial \boldsymbol{Q}$ the species elements of $\boldsymbol{C}_{i,j}$ forms a lower triangular matrix.

The LU-factored form of the preceding equations becomes

$$\boldsymbol{L}\boldsymbol{D}^{-1}\boldsymbol{U} = -\mathbf{RHS} \tag{16}$$

$$\boldsymbol{D} = \boldsymbol{C}_{i,j}, \qquad \boldsymbol{L} = \boldsymbol{C}_{i,j} + \boldsymbol{C}_{i-1} + \boldsymbol{C}_{j-1}$$

$$\boldsymbol{U} = \boldsymbol{C}_{i,j} + \boldsymbol{C}_{i+1} + \boldsymbol{C}_{j+1} \tag{17}$$

In the partially implicit scheme the species elements of the diagonal matrix $\boldsymbol{D}$ forms a lower triangular matrix, and thus it is possible to invert the diagonal term of the Eq. (14a) faster than the fully implicit scheme by one order of magnitude. The partially implicit scheme does not affect the steady-state solution because the **RHS** term goes to zero if the solution converges.

Results

Shock-Induced Combustion

Shock-induced combustion around a blunt body is considered as an example of supersonic reacting flows. The experimental conditions of Lehr[7] are used for the present calculation. Initial pressure and temperature are 186 mmHg and 292 K, respectively. The projectile's flight Mach number is 3.55 in the stoichiometric hydrogen–oxygen mixture. The diameter of the projectile is 15 mm. For the combustion model a six-species and eight-reaction-steps model[17] is used. The local time-stepping method is employed on a 60×100 grid, with a Courant–Friedrichs–Lewy (CFL) number of 7. For this supersonic case the preconditioning parameter ε_p is set to be one. For the first 10 iterations the CFL number is fixed to be 0.1 to ensure stable computation. Thus the CFL number is gradually increased to seven.

Figure 3 shows the density contours predicted by the fully implicit scheme compared with experimental shadowgraphs.[7] The computed shock position and reaction front show good agreement with the experimental results. The results of partially and diagonally implicit schemes are identical to that of the fully implicit one; therefore, those are not presented. The convergence histories of the three methods are presented in Fig. 4. The convergence history of the partially implicit scheme is nearly identical to that of the fully implicit one, but the diagonal scheme shows a stagnant behavior after converging to a certain error level. Relative to the fully implicit scheme, the partially implicit scheme saves computational time per iteration by about 20%.

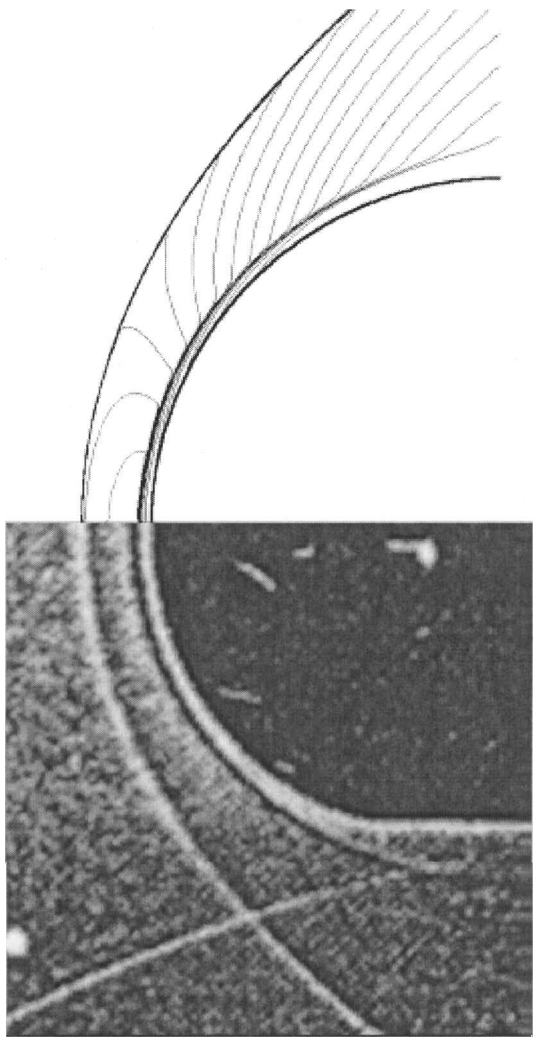

Fig. 3 Density contours of the converged solution on a 60×100 grid compared with Lehr's shadowgraph.[7]

Planar Reacting Shear Layer

The planar reacting shear layer of Chang et al.[8] is calculated as an example of subsonic reacting flows. Here, the lower airstream conditions are $U_1 = 390$ m/s and $T_1 = 811$ K. The upper stream is composed of 96.06% N_2 and 3.94% H_2 by mass with $U_2 = 140$ m/s and $T_2 = 366.5$ K. A hydrogen torch is implemented to sustain combustion. The condition at the centerline with 1-mm width are $T = 1250$ K, 77.7% N_2, 1.3% H_2, 21% O_2, and $U_3 = 140$ m/s. The corresponding Mach numbers of the two streams are 0.68 and 0.4, respectively. For the reaction mechanism the GRI nine-species and 25-reaction-steps model is used. The CFL number is 30 in the linear convergence regimes, and the grid density is 65×65 with clustering near the centerline. The computed velocity profiles are compared with experimental data at several locations from the splitter edge in Fig. 5. The spreading rate is underpredicted, as in earlier studies.[6,12]

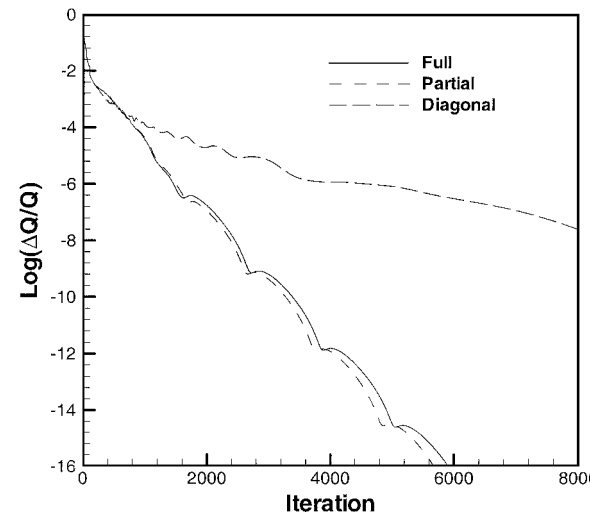

Fig. 4 Convergence histories of shock-induced combustion on a 60×100 grid. (CFL number is seven, and the local time step is used.)

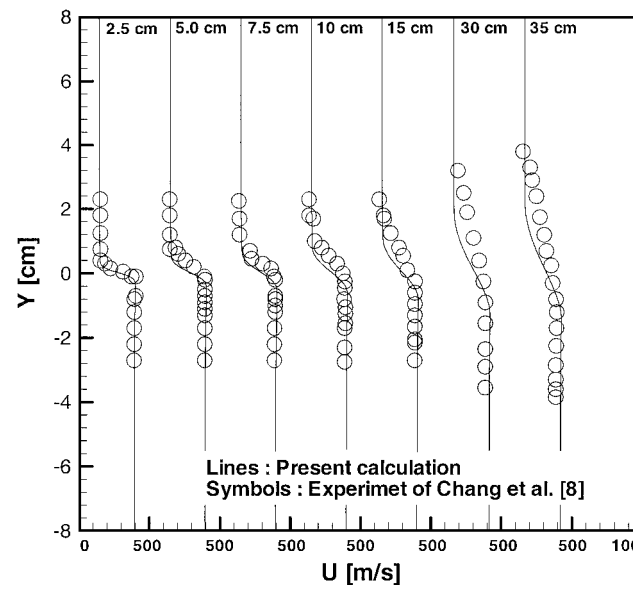

Fig. 5 Axial velocity profiles of the reacting shear layer on the 65×65 grid.

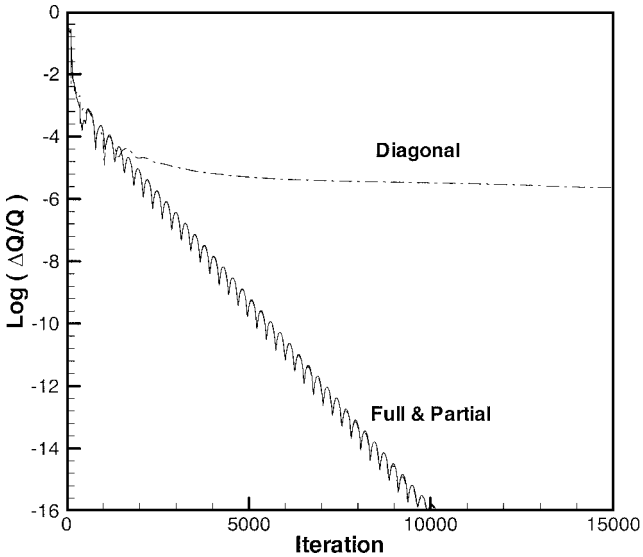

Fig. 6 Convergence histories of the fully, partially, and diagonally implicit schemes for a planar reacting flow.

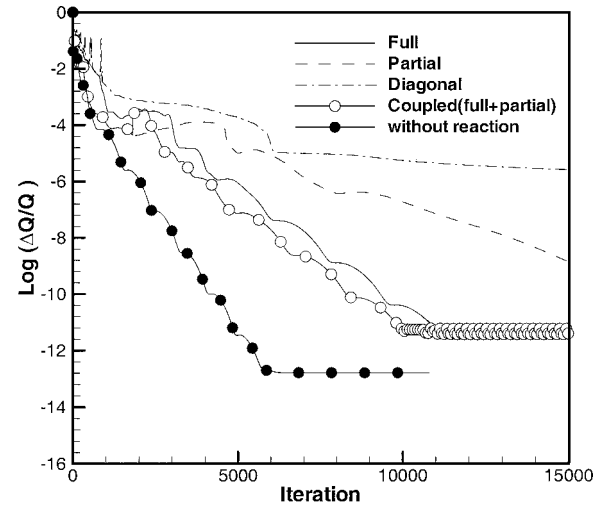

Fig. 8 Convergence histories of computations of frozen and reacting flows with the fully, partially, diagonally, and coupled (fully and partially) implicit schemes for hydrogen-air diffusion flame. The local time step is used on a 60 × 50 grid.

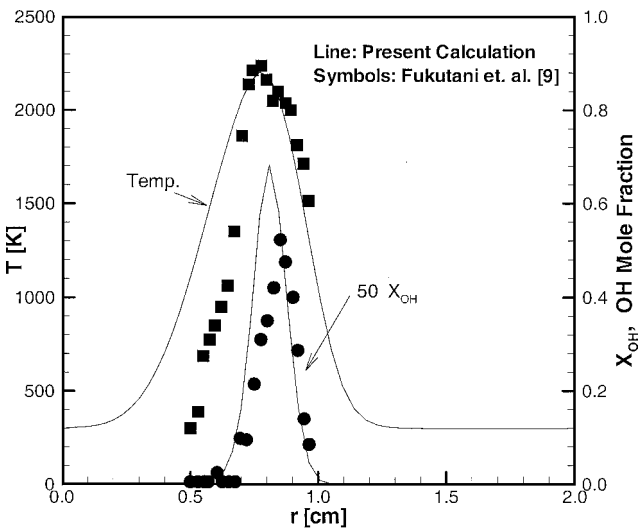

Fig. 7 Comparison of the computed OH mole fraction and temperature profiles with the data from Fukutani et al.[9] at 2 mm from the nozzle.

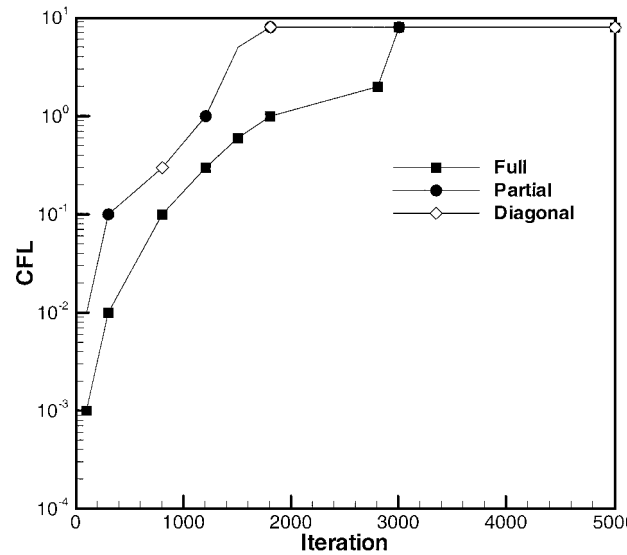

Fig. 9 CFL numbers of the fully, partially, and diagonally implicit schemes in the computation of a hydrogen-air diffusion flame.

Figure 6 shows the convergence histories of three schemes. The partially implicit scheme shows the same convergence rate as the fully implicit one, but the diagonal scheme shows a stagnant behavior. Such convergence characteristics are similar to those of shock-induced combustion. In this case the partially implicit scheme reduces computing time by approximately 8%.

Laminar Diffusion Flames

As an additional example of subsonic flows, hydrogen-air diffusion flames are considered. The hydrogen air flame is calculated for the experimental conditions of Fukutani et al.[9] Hydrogen is injected at a rate of 34 ml/s from a 1-cm-diam nozzle, and the airflow rate from a 4-cm-diam nozzle is 340 ml/s. The Mach number of the fuel jet is 2.9×10^{-4}. The GRI 9-species and 25-reaction-step model is used. For the ignition the fuel temperature is fixed to 2000 K at the first iteration. Although several other methods of ignition are performed, similar convergence behaviors to the present one were observed. The transport properties are calculated every three iterations in order to save computing time.

Figure 7 shows the measured and the predicted temperatures and OH mole fractions. The discrepancies in the fuel side can be noted, and these are also observed in the calculation of Fukutani et al.,[9] which may be caused by lip thickness or inaccurate inlet conditions. Despite the differences, the predictions show satisfactory agreement with the experimental data.

Figure 8 shows the convergence histories of the fully, partially, and diagonally implicit schemes compared with those for a nonreacting flow. The convergence rate of the partially implicit scheme is slower than that of the fully implicit one, and there appears long nonlinear initial behavior regardless of the schemes. During this nonlinear period, the CFL numbers are severely restricted as shown in Fig. 9. However, after this period the CFL number recovers to the optimum value of eight, and the convergence rates show nearly linear behaviors. In the linear stage the convergence rate of the partially implicit scheme is slower than that of the fully implicit scheme. However, during the nonlinear phase the partially implicit scheme can enhance numerical stability by alleviating the time-step limitation. The allowed time-step sizes of the partially implicit scheme are 10 times larger than those of the fully implicit one. Such behavior coincides with the results of the constant volume reaction, in which the calculation with the partial chemical Jacobian allows larger time-step sizes. Therefore, the partially implicit scheme is robust in the presence of strong chemical reactions.

Such enhanced robustness suggests that more stable and efficient computations are possible when the fully implicit scheme is coupled with the partially implicit one. As an example, the computation is performed with the partially implicit scheme for the first 1800 iteration numbers and then proceeds with the fully implicit one. As shown in Fig. 8, this coupled implicit scheme is able to calculate chemical reactions more robustly than the fully implicit scheme during the initial nonlinear stage. The coupled scheme shows the same convergence rate during the linear stage and thus reduces the total computing time by approximately 15%. This saving rate, however, decreases if the transport properties are calculated at every iteration.

The partially implicit scheme was applied to more complicated reaction mechanisms by calculating a laminar methane-air diffusion flame involving a chemical Jacobian matrix of high dimension. The methane-air diffusion flame calculation is conducted under the condition of Mitchell et al.[10] Methane is injected at the rate of 5.7 cc/s from a 0.653-cm-diam nozzle, and the airflow rate from a 2.54-cm-diam nozzle is 187.7 cc/s. The Mach number of the fuel jet is 10^{-4}. The reaction model consists of 17 species 58 reaction steps of Bilger et al.[18] The carbon compound species are located in the front side of the primary dependent vector.

Figure 10 shows the measured and the predicted temperatures and the mole fractions of some species. The discrepancies in the air side are also observed in the calculation of Venkateswaran et. al.[6] Figure 11 shows the convergence histories and CFL numbers of the fully implicit scheme and the partially implicit scheme coupled with the fully implicit scheme. Nonlinear initial behavior is observed as in the hydrogen-air flame. In this computation the partially implicit scheme is changed to the fully implicit scheme after 900th iteration. The time-step sizes of the partially implicit scheme during initial iterations, shown in Fig. 11, are larger than those of the fully implicit scheme. Thus, the robustness of the partially implicit scheme is evident. With the coupled scheme the total computing time is reduced by 15%.

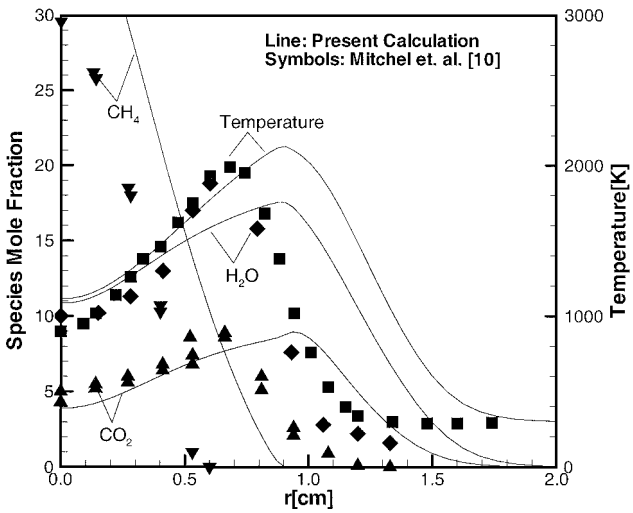

Fig. 10 Experimental data[10] and prediction with Bilger et al.'s 58-reaction-steps model[18] for a methane-air diffusion flame.

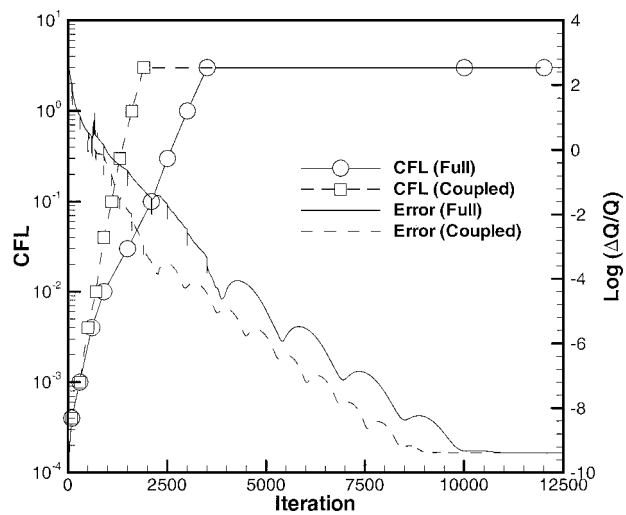

Fig. 11 CFL numbers and convergence histories of the fully and coupled implicit schemes for a methane-air diffusion flame.

Conclusions

For efficient and stable computation of chemically reacting flows, a partially implicit scheme has been developed and applied to various reacting flows ranging from subsonic to supersonic flows in conjunction with the time-derivative preconditioned equations. The partially implicit scheme has the advantage of mitigating the chemical stiffness and thus allows stable computation and larger time-step sizes.

Its performance depends on the flow Mach number. In high-Mach-number flows such as shock-induced combustion and planar reacting flows, the partially implicit scheme has the nearly identical convergence characteristics with the fully implicit scheme and thus can save computational time caused by efficient matrix inversion. On the other hand, in low-Mach-number flows the convergence rate of the partially implicit scheme rather slows down compared with that of the fully implicit scheme. However, the partially implicit scheme can still alleviate the strong chemical stiffness, and this robustness allows less-restricted time-step sizes in the initial stages of the reactions. Furthermore, more robust and efficient computations are possible if the fully implicit scheme is coupled with the partially implicit one.

Acknowledgments

The authors gratefully acknowledge support from the Korea Science and Engineering Foundation, KOSEF 98-0200-04-01-3 and BK-21. The authors express sincere gratitude to S. J. Song for his technical English editing.

References

[1]Merkle, C. L., Venkateswaran, S., and Deshpande, M., "Efficient Implementation of Turbulence Modeling in Computational Schemes," 2nd National Congress on Computational Mechanics, Washington, DC, 1993.

[2]Yoon, S., and Jameson, A., "Lower-Upper Symmetric-Gauss-Seidel Method of the Euler and Navier–Stokes Equations," *AIAA Journal*, Vol. 26, No. 9, 1988, pp. 1025, 1026.

[3]Eberhardt, S., and Imlay, S., "Diagonal Implicit Scheme for Computing Flows with Finite Rate Chemistry," *Journal of Thermophysics and Heat Transfer*, Vol. 6, No. 2, 1992, pp. 208–216.

[4]Edwards, J. R., "An Implicit Multigrid Algorithm for Computing Hypersonic, Chemically Reacting Viscous Flows," *Journal of Computational Physics*, Vol. 123, No. 1, 1996, pp. 84–95.

[5]Kim, S.-L., Jeung, I.-S., Park, Y.-H., and Choi, J.-Y., "Approximate Chemical Jacobian Method for Efficient Calculation of Reactive Flows," AIAA Paper 2000-3384, July 2000.

[6]Venkateswaran, S., Despande, M., and Merkle, C. L., "The Application of Preconditioning to Reacting Flow Computations," AIAA Paper 95-1673, 1995.

[7]Lehr, H. F., "Experiment on Shock-Induced Combustion," *Astronautica Acta*, Vol. 17, Nos. 4 and 5, 1972, pp. 589–797.

[8]Chang, C. T., Marek, C. J., Wey, C., Jones, R. A., and Smith, M. J., "Comparison of Reacting and Non-Reacting Shear Layers at High Subsonic Mach Number," AIAA Paper 93-2381, June 1993; also NASA TP-3342, June 1996.

[9]Fukutani, S., Kunioshi, N., and Jinno, H., "Flame Structure of an Axisymmetric Hydrogen-Air Diffusion Flame," *Proceedings of the Combustion Institute*, Vol. 23, 1990, pp. 567–573.

[10]Mitchell, R. E., Sarofim, A. F., and Clomburg, L. A., "Experimental and Numerical Investigation of Confined Laminar Diffusion Flames," *Combustion and Flame*, Vol. 37, No. 3, 1980, pp. 227–244.

[11]Shuen, J.-S., Chen, K.-H., and Choi, Y.-H., "A Coupled Implicit Methods for Chemical Non-equilibrium Flows at All Speeds," *Journal of Computational Physics*, Vol. 106, No. 2, 1993, pp. 306–318.

[12]Edwards, J. R., and Roy, C. J., "Preconditioned Multigrid Methods for Two-Dimensional Combustion Calculation at All Speeds," *AIAA Journal*, Vol. 36, No. 2, 1998, pp. 185–192.

[13]Choi, Y.-H., and Merkel, C. L., "The Application of Preconditioning in Viscous Flows," *Journal of Computational Physics*, Vol. 105, No. 2, 1993, pp. 207–223.

[14]Roe, P. L., "Approximate Riemann Solvers, Parameter Vectors, and Difference Schemes," *Journal of Computational Physics*, Vol. 43, No. 2, 1981, pp. 357–372.

[15]Buelow, P. E. O., "Convergence Enhancement of Euler and Navier–Stokes Algorithms," Ph.D. Dissertation, Dept. of Mechanical Engineering, Pennsylvania State Univ., University Park, PA, 1995.

[16]Montagne, J. L., Yee, H. C., Klopfer, G. H., and Vinokur, M., "Hypersonic Blunt Body Computation Including Real Gas Effects," NASA TM 10074, March 1988.

[17]Evans, J. S., and Schexnayder, C. J., "Influence of Chemical Kinetics and Unmixedness on Burning in Supersonic Hydrogen Flames," *AIAA Journal*, Vol. 18, No. 2, 1980, pp. 188–193.

[18]Bilger, R. W., Starner, S. H., and Kee, R. J., "On Reduced Mechanism for Methane-Air Combustion in Nonpremixed Flames," *Combustion and Flame*, Vol. 80, No. 2, 1990, pp. 135–149.

K. Kailasanath
Associate Editor